The cell adhesion molecule IGPR-1 is activated by and regulates responses of endothelial cells to shear stress

Received for publication, March 20, 2019, and in revised form, July 19, 2019 Published, Papers in Press, July 24, 2019, DOI 10.1074/jbc.RA119.008548

Rachel Xi-Yeen Ho[‡], **Rawan Tahboub**[‡], **Razie Amraei**[‡], **Rosana D. Meyer**[‡], **Nitinun Varongchayakul**[§], **Mark Grinstaff**[§], and **Nader Rahimi**[‡1]

From the [‡]*Department of Pathology, School of Medicine, Boston University Medical Campus, Boston, Massachusetts 02118 and the* [§]*Departments of Biomedical Engineering, Chemistry, and Medicine, Boston University, Boston, Massachusetts 02215*

Edited by Alex Toker

Vascular endothelial cells respond to blood flow-induced shear stress. However, the mechanisms through which endothelial cells transduce mechanical signals to cellular responses remain poorly understood. In this report, using tensile-force assays, immunofluorescence and atomic force microscopy, we demonstrate that immunoglobulin and proline-rich receptor-1 (IGPR-1) responds to mechanical stimulation and increases the stiffness of endothelial cells. We observed that IGPR-1 is activated by shear stress and tensile force and that flow shear stress–mediated IGPR-1 activation modulates remodeling of endothelial cells. We found that under static conditions, IGPR-1 is present at the cell–cell contacts; however, under shear stress, it redistributes along the cell borders into the flow direction. IGPR-1 activation stimulated actin stress fiber assembly and cross-linking with vinculin. Moreover, we noted that IGPR-1 stabilizes cell–cell junctions of endothelial cells as determined by staining of cells with ZO1. Mechanistically, shear stress stimulated activation of AKT Ser/Thr kinase 1 (AKT1), leading to phosphorylation of IGPR-1 at Ser-220. Inhibition of this phosphorylation prevented shear stress–induced actin fiber assembly and endothelial cell remodeling. Our findings indicate that IGPR-1 is an important player in endothelial cell mechanosensing, insights that have important implications for the pathogenesis of common maladies, including ischemic heart diseases and inflammation.

Endothelial cells shelter the internal surface of blood vessels, maintain vascular and tissue homeostasis, and modulate many key physiological processes, including angiogenesis, immune responses, and dynamic fluid exchanges throughout organs. Homeostasis of endothelial cells necessitates the assimilation of various signals from sites of adhesion to extracellular matrix components and adjacent cells, signals from circulating soluble factors, as well as mechanical stimuli (1). The conversion of mechanical forces into biochemical signals is fundamental to the development of the vascular system and function (2). Highly specific molecular interactions, typically by cell surface receptors known as cell adhesion molecules (CAMs)[2] (*e.g.* integrins and cadherins), mediate the conversion of mechanical forces into biochemical signals to control a wide range of biological processes. CAMs such as cadherins, which are involved in cell–cell interaction, function as mechanosensors at cell–cell junctions (3, 4), whereas integrins function as the mechanotransducers between the extracellular matrix and the actomyosin cytoskeleton (5). Interestingly, although vascular endothelial cadherin is involved in mechanosensor signaling, it does not appear to be a direct mechanotransducer (4, 6). The incorporation, transmission, and governance of mechanical stimuli at sites of adhesion is of fundamental importance because they drive blood vessel development and are key players of cardiovascular disease progression (7).

Immunoglobulin and proline-rich receptor-1 (IGPR-1, also called TMIGD2) is a newly identified CAM that plays an important role in the adhesion of endothelial cells (8). In addition, IGPR-1 supports the growth of colon cancer cell lines by promoting multicellular aggregation in the absence of adhesion to substratum (9). IGPR-1 transmits intracellular information in part by interacting with several Src homology 3 domain containing proteins such Src homology 3 protein interacting with Nck90 (SPIN90, also called WISH/NCKIPSD) (8). Inhibition of transhomophilic dimerization of IGPR-1 by deletion of the extracellular domain or by a blocking antibody impairs its ability to regulate endothelial barrier function (10). This underscores the importance of the extracellular domain of IGPR-1 in its activation. IGPR-1 localizes to endothelial adherent junctions, and its activation via transhomophilic dimerization stimulates phosphorylation of Ser-220 (10). In this study, we report that IGPR-1 functions as a mechanosensitive receptor that is activated by shear stress and plays a critical role in endothelial cell response to flow shear stress.

This work was supported in part by NCI, National Institutes of Health Grants R21CA191970 and R21CA193958 and Clinical and Translational Science Institute Grant 1UL1TR001430 (to N. R.).The authors declare that they have no conflicts of interest with the contents of this article. The content is solely the responsibility of the authors and does not necessarily represent the official views of the National Institutes of Health.
This article contains Table S1 and Figs. S1–S6.

[1] To whom correspondence should be addressed: Dept. of Pathology, Boston University Medical Campus, Boston, MA 02118. Tel.: 617-358-2432; Fax: 617-414-7914; E-mail: nrahimi@bu.edu.

[2] The abbreviations used are: CAM, cell adhesion molecule; IGPR, immunoglobulin and proline-rich receptor; AFM, atomic force microscopy; PAE, porcine aortic endothelial; EV, empty vector; HUVEC, human umbilical venous endothelial cell; DMEM, Dulbecco's modified Eagle's medium; DAPI, 4′,6′-diamino-2-phenylindole; GAPDH, glyceraldehyde-3-phosphate dehydrogenase.

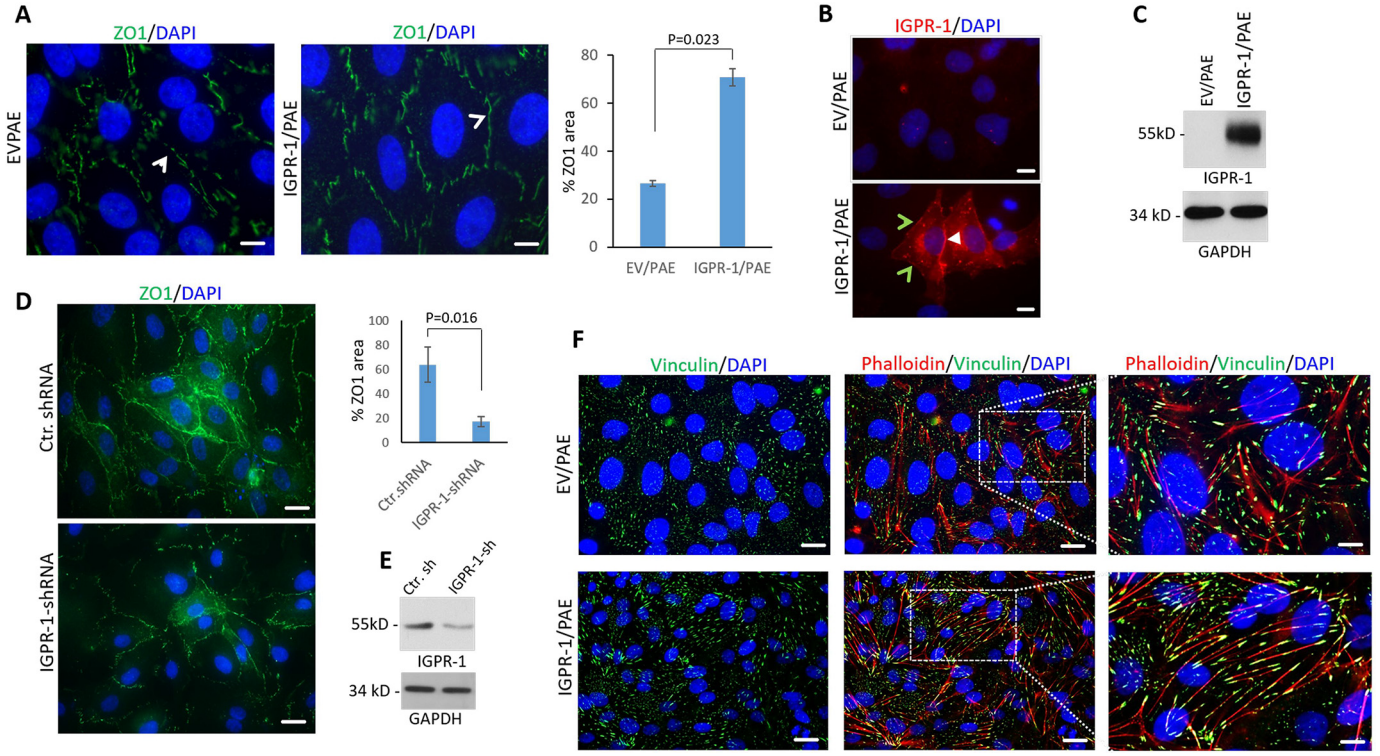

Figure 1. IGPR-1 stabilizes cell–cell junctions and stimulates actin stress fiber assembly. *A*, PAE cells expressing EV or IGPR-1 were stained with anti-ZO1 antibody (*green*) and DAPI (*blue*). An *arrowhead* indicates ZO1 staining at cell junctions. The ImageJ program was used to quantify ZO1 staining (four field/group). *B*, the same cells were also stained with anti–IGPR-1 antibody (*red*) and DAPI for nucleus (*blue*). A *white arrowhead* shows IGPR-1 expression in cell–cell contact area. *Green arrowheads* point to expression of IGPR-1 when cells are not in contact with each other. Image magnification, 10 μm. *C*, ectopic expression of IGPR-1 in PAE cells. *D*, HUVECs expressing control (*Ctr.*) shRNA or IGPR-1–shRNA were stained for ZO1 and DAPI. Quantification of ZO1 staining is shown (four fields/group). *E*, knockdown of IGPR-1 in HUVECs. Whole-cell lysates expressing control shRNA (*Ctr.sh*) or IGPR-1–shRNA (*IGPR-1-sh*) was blotted with anti–IGPR-1 antibody or anti-GAPDH antibody for loading control. *F*, IGPR-1/PAE and EV/PAE cells were stained with phalloidin (*red*) for actin, anti-vinculin (*green*), and DAPI (*blue*). *Scale bar*, 10 μm.

Results

IGPR-1 induces adherens junction assembly in endothelial cells

In response to various physical and chemical stimuli, endothelial cells undergo morphological remodeling and cytoskeletal actin stress fiber rearrangements (11, 12), which involve cross-linking vinculin with actin filaments. This cross-linking of vinculin with actin filaments is a critical step for formation of focal adhesions and also in capping actin filaments to regulate actin dynamics (13) that is critical for the mechanical strength of focal adhesions (14). Our recent work indicated that IGPR-1 is present at the endothelial adherens junctions and potentially plays a role in angiogenesis and stabilization of vessels (8, 10).

To assess the role of IGPR-1 in endothelial cell adherens junction, we stained porcine aortic endothelial (PAE) cells expressing empty vector (EV) or IGPR-1 for ZO1 (zonula occluden 1). ZO1 is a scaffolding protein that links transmembrane proteins at the cell junction to the actin cytoskeleton, which is also required for endothelial adherens junction and barrier function (15, 16). IGPR-1 increased stability of endothelial cell adherens junctions as determined by immunostaining of PAE cells with ZO1 (Fig. 1*A*). Staining of IGPR-1/PAE cells with anti–IGPR-1 antibody showed that IGPR-1 was preferentially localized at the periphery of the endothelial cell–cell contacts (Fig. 1*B*). Ectopic expression of IGPR-1 in PAE cells also was confirmed by Western blotting (Fig. 1*C*). Next, we asked whether silencing IGPR-1 in human umbilical venous endothelial cells (HUVECs) affects adherens junctions. Knockdown of IGPR-1 in HUVECs by shRNA considerably decreased adherens junctions (Fig. 1*D*). The knockdown of IGPR-1 by shRNA in HUVECs is shown (Fig. 1*E*). Re-expressing IGPR-1 in these cells rescued stability of adherens junctions as determined by staining of cells with ZO1 (Fig. S1*B*).

IGPR-1 expression in PAE cells also markedly increased actin stress fiber networks and stimulated cross-linking of vinculin with actin filaments (Fig. 1*F*). Taken together, the data indicate that IGPR-1 increases tight junction formation as determined by ZO1 staining and actin architecture reorganization into stress fiber arrays as determined by phalloidin staining.

Endothelial cell spreading and density activates IGPR-1

Given that the stability of cell–cell junctions and actin stress fiber dynamics are modulated by cell spreading and adhesion (17), we examined the role of cell spreading and cell–cell contact in the activation of IGPR-1. To test the role of cell spreading in activation of IGPR-1, IGPR-1/PAE cells were seeded and allowed to adhere for various time points (1–4 h), and activation of IGPR-1 was determined by Western blotting using a previously validated pSer-220 antibody (10). Within 1 h, as cells began to adhere and spread (Fig. 2*A*), phosphorylation of IGPR-1 at Ser-220 was significantly increased and remained phosphorylated for up to 4 h as cells became fully adhered

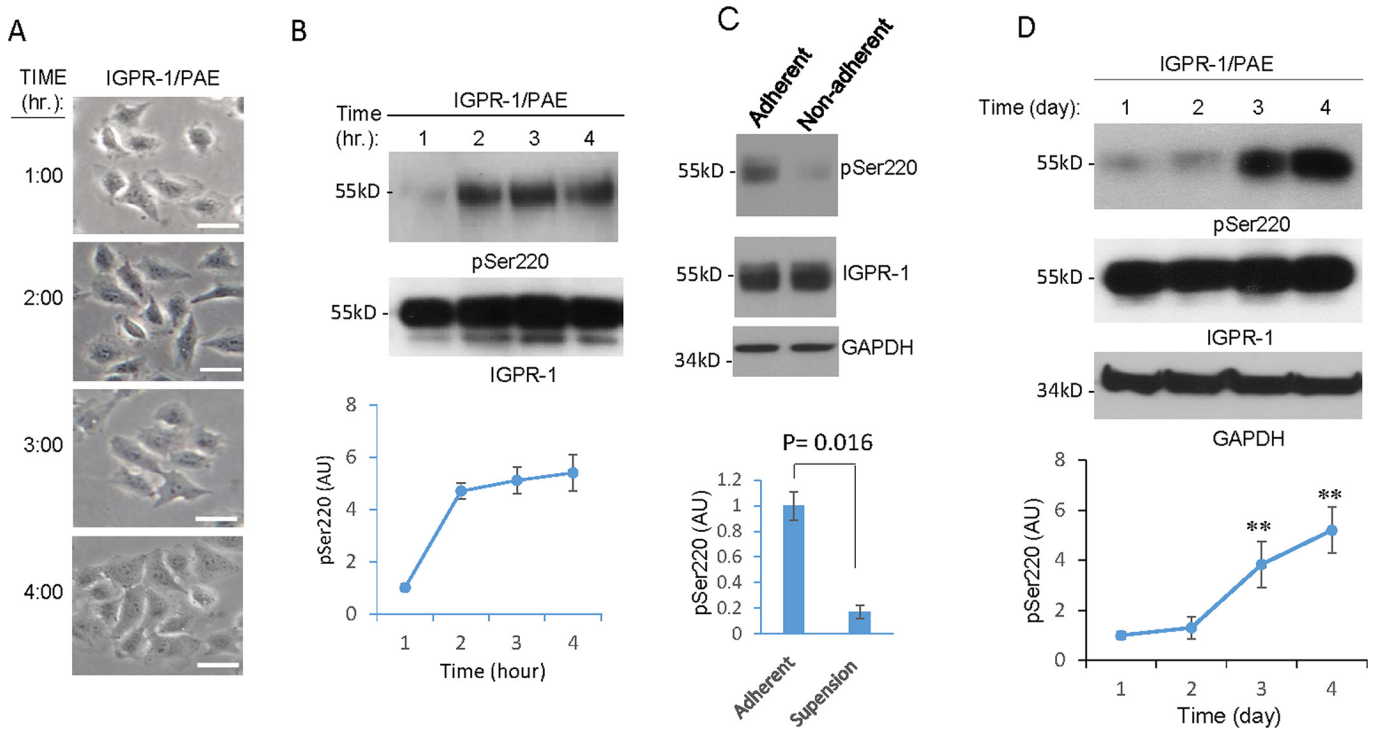

Figure 2. Endothelial cell spreading and density regulate phosphorylation of IGPR-1. *A*, IGPR-1/PAE cells were plated on 60-mm plates for the indicated times (1–4 h). The pictures were taken under microscope before cells were lysed. *B*, whole-cell lysates were blotted with anti–pSer-220 antibody (*pSer200*) or total IGPR-1. The graph is representative of three independent experiments. *C*, IGPR-1/PAE cells were seeded in adherent or in low adherent cell culture plates for 1 h. The cells were lysed, and whole-cell lysates were blotted for pSer-220, total IGPR-1, and GAPDH. *D*, IGPR-1/PAE cells were seeded in sparse conditions (40–50% confluence) and were lysed at day 1, 2, 3, or 4. Whole-cell lysates were blotted for pSer-220, total IGPR-1, and GAPDH. The graph is representative of three independent experiments. **, $p < 0.01$.

(Fig. 2*B*). However, IGPR-1 was not phosphorylated when cells were seeded on the low attachment plates (*i.e.* suspension), which prevents cell spreading (Fig. 2*C*), indicating that cell spreading is required for IGPR-1 activation.

To demonstrate the role of cell density in IGPR-1 activation, the cells were plated in a sparse (40–50% confluent) condition, which reached full confluency at days 3 and 4. Phosphorylation of IGPR-1 in normalized whole-cell lysates was assessed by Western blotting analysis. The basal level of Ser-220 phosphorylation was determined at days 1 and 2 (Fig. 2*D*). As confluency of cells increased, phosphorylation of IGPR-1 was also significantly augmented (1.3-fold at day 2, 3.9-fold at day 3, and 5.2-fold at day 4) (Fig. 2*D*). The cell density–dependent phosphorylation of IGPR-1 was inhibited when IGPR-1/PAE cells were mixed (1:1 ratio) with PAE cells expressing empty vector (EV/PAE) (Fig. S2*A*), indicating that cell density–dependent IGPR-1 phosphorylation is associated with its transdimerization. In support of this possibility, incubation of IGPR-1/PAE cells with a blocking antibody (1A12) inhibited cell density–dependent phosphorylation of IGPR-1 (Fig. S1*B*).

AKT stimulates phosphorylation of IGPR-1 at Ser-220

Considering that IGPR-1 phosphorylation at Ser-220 is regulated by cell adhesion (Fig. 2*B*) and along with our previous observation that AKT phosphorylates IGPR-1 at Ser-220 in colon cancer cell line HCT116 (9), we asked whether AKT is activated in a cell adhesion–dependent manner in PAE cells. We found AKT was phosphorylated in PAE cells in a cell adhesion–dependent manner (Fig. 3*A*), suggesting a possible link between activation of AKT and phosphorylation of IGPR-1 at Ser-220. In that regard, we examined the role of AKT in the phosphorylation of IGPR-1 in endothelial cells.

For this, we asked whether overexpression of a dominant-negative AKT1 (K179M/T308A/S473A) can inhibit IGPR-1 phosphorylation. Western blotting analysis demonstrated that expression of K179M/T308A/S473A-AKT inhibited Ser-220 phosphorylation of IGPR-1 (Fig. 3*B*). Furthermore, treatment of IGPR-1/PAE cells and HUVECs endogenously expressing IGPR-1 with an AKT inhibitor, GSK-690693 (4 nM, 60 min), also effectively inhibited phosphorylation of IGPR-1 at Ser-220 (Fig. 3, *C* and *D*). Taken together, our data demonstrate that AKT mediates phosphorylation IGPR-1 at Ser-220.

Shear stress promotes actin remodeling and cell realignment in IGPR-1–dependent manner

Previous studies have shown that in response to fluid flow, endothelial cells align along the direction of fluid flow (19). We asked whether shear stress modulates localization of IGPR-1 in endothelial cells. In static conditions, IGPR-1 was localized indiscriminately at the cell–cell contact regions. However, under shear stress, IGPR-1 was distributed laterally along the direction of flow (Fig. 4*A*). Another known response to shear stress is the remolding of the actin cytoskeleton, which produces various cellular responses and activates several major signaling proteins (20, 21). We asked whether IGPR-1 mediates changes in the actin cortex network and cell realignment induced by flow shear stress. Under flow shear stress, IGPR-1/PAE cells exhibited extensive and robust actin cortex network

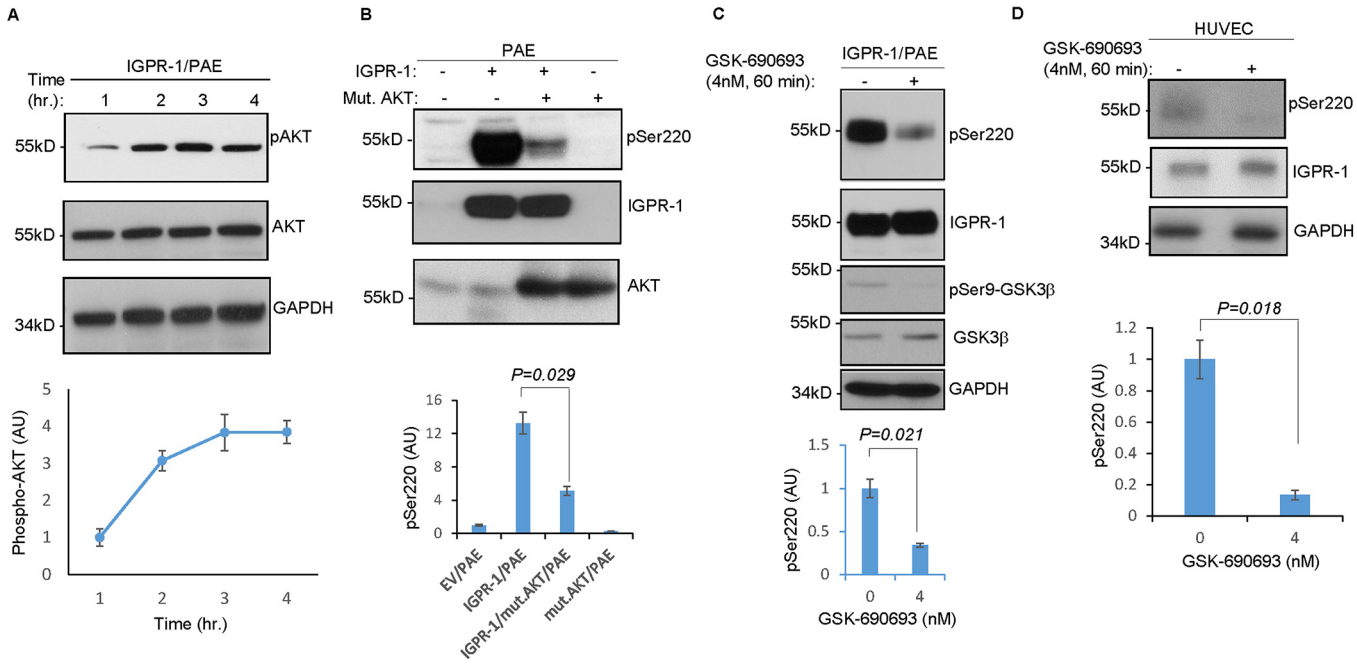

Figure 3. AKT mediates phosphorylation of IGPR-1 at Ser-220. *A*, equal number of PAE cells expressing IGPR-1 were seeded on the cell culture plates for various time points. The cells were lysed, and whole-cell lysates were blotted for phospho-AKT, total AKT, and GAPDH. The graph is representative of three independent experiments. *B*, equal number of PAE cells expressing EV or IGPR-1 alone or co-expressed with mutant dominant-negative AKT1 (K179M/T308A/S473A) were lysed, and whole-cell lysates were blotted for pSer-220 (*pSer220*), total IGPR-1, and AKT. *C*, IGPR-1/PAE cells were treated with control vehicle or GSK-690693 for 60 min, the cells were lysed, and whole-cell lysates were blotted for pSer-220, total IGPR-1, pSer-9–GSK3β, total GSK3β, and GAPDH. The graph is representative of three independent experiments. pSer-220 level is normalized to total IGPR-1. *D*, HUVECs were treated with control vehicle or GSK-690693 for 60 min, and whole-cell lysates were blotted for pSer-220, total IGPR-1, or GAPDH. The graph is pSer-220 level normalized to total IGPR-1, which is representative of three independent experiments. *Mut.* or *mut.*, mutant.

along the direction of flow shear stress, with ring-like F-actin structures compared with normal static conditions (Fig. 4*B*). However, actin cortex networks in the control PAE (EV/PAE) cells under identical flow shear stress conditions were concentrated mainly at the periphery of the cells (Fig. 4*D*). We also quantified F-actin orientation (*i.e.* anisotropy) and F-actin expression (*i.e.* mean fluorescence intensity) using an open source plugin for ImageJ, Fibriltool software (22), which shows a significant increase in both actin fluorescence intensity and orientation in IGPR-1/PAE cells (Fig. 4*B*, *lower panel*). Actin fluorescence intensity and orientation under shear stress did not significantly change in PAE cells expressing empty vector (Fig. 4*D*). As noted, IGPR-1/PAE cells also underwent a significant realignment in response to flow compared with control PAE cells expressing empty vector, EV/PAE (Fig. 4, *C* and *E*). The data demonstrate that IGPR-1 modulates endothelial cells' response to shear stress.

Shear stress stimulates phosphorylation of IGPR-1 through activation of AKT

Blood vessels are subject to shear stress caused by blood flow and are able to respond to changes in flow by translating mechanical stimuli into intracellular signals (23). IGPR-1 is expressed in both arterial and venous endothelial cells (Fig. S3, *A* and *B*), and considering its role in endothelial cells' response to shear stress (Fig. 4*B*), we examined whether IGPR-1 is activated by shear stress. We subjected HUVECs to shear stress and measured phosphorylation of IGPR-1 at Ser-220. Phosphorylation of IGPR-1 increased by nearly 4-fold in response to shear stress (Fig. 5*A*). Similarly, phosphorylation of IGPR-1 in IGPR-1/PAE cells subjected to flow shear stress was strongly increased within 30 min and remained phosphorylated at 60 min (Fig. 5*B*).

Phosphatidylinositol 3-OH-kinase (6) and its downstream serine/threonine kinase, AKT1, are activated in response to flow shear stress (24, 25), and given that AKT also phosphorylates IGPR-1 at Serine 220, we probed whether shear stress–induced phosphorylation of IGPR-1 at Ser-220 is mediated by AKT. Consistent with the previous observations, flow shear stress induced AKT1 activation (Fig. S4*A*). Additionally, expression of IGPR-1 in PAE cells, increased phosphorylation of AKT1 (Fig. S4*A*), and co-expression of a dominant-negative AKT1 with IGPR-1 inhibited shear stress– and IGPR-1–dependent phosphorylation of AKT1 (Fig. S4*A*).

To address the flow shear stress–induced activation of AKT1 in IGPR-1 phosphorylation, we measured IGPR-1 phosphorylation in PAE cells treated with the AKT inhibitor GSK-690693 under shear stress. GSK-690693 inhibited shear stress–induced phosphorylation of IGPR-1 (Fig. 5*C*). Moreover, co-expression of dominant-negative AKT1 with IGPR-1 also inhibited shear stress–induced phosphorylation of IGPR-1 at Ser-220 (Fig. 5*D*). Furthermore, co-expression of the dominant-negative AKT1 with IGPR-1 considerably inhibited the flow shear stress–induced actin stress fiber rearrangement and cell realignment of PAE cells (Fig. 5*E*).

To investigate whether Ser-220 phosphorylation of IGPR-1 is important for actin stress fiber network assembly and realignment of endothelial cells in response to shear stress, we generated PAE cells expressing A220/IGPR-1 (A220–IGPR-1/PAE,

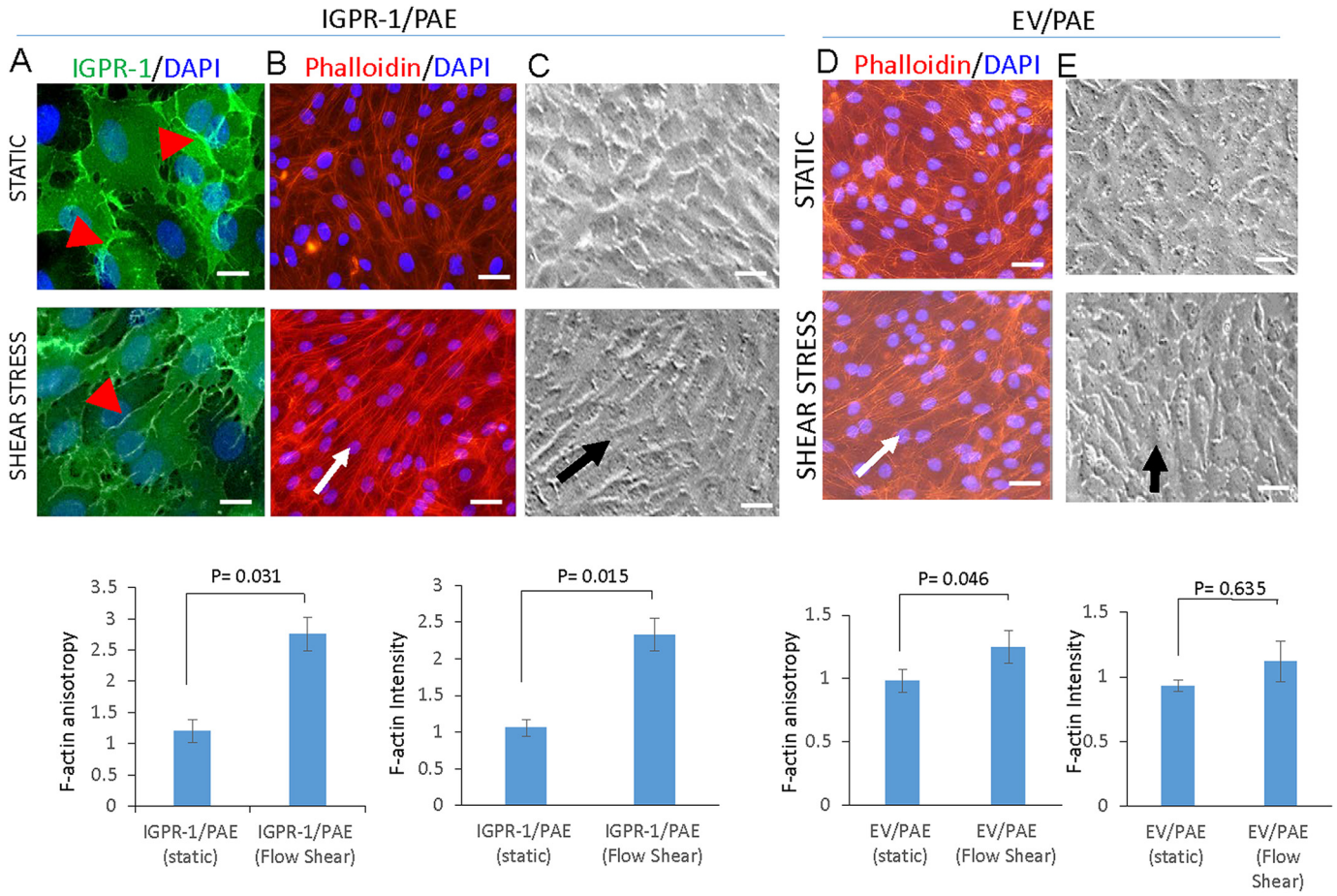

Figure 4. IGPR-1 regulates shear stress–induced actin stress rearrangement. *A*, IGPR-1/PAE cells incubated under normal static or shear stress conditions. The cells were fixed and stained with anti–IGPR-1 antibody. *Arrowheads* show differential localization of IGPR-1 under static *versus* shear stress. *B*, IGPR-1/PAE cells under similar conditions were stained with phalloidin for actin (*red*) and DAPI (*blue*). F-actin orientation (anisotropy) and expression were quantified using an open source plugin Fibriltool for ImageJ. *C*, morphology of IGPR-1/PAE cells under normal static and shear stress is shown. The *arrow* shows the direction of the flow. *D*, EV/PAE cells kept in normal static or under shear stress conditions were fixed and then stained with phalloidin for actin (*red*) and DAPI (*blue*). F-actin orientation (anisotropy) and expression was quantified using an open source plugin Fibriltool for ImageJ. *E*, morphology of EV/PAE cells under normal static and shear stress conditions are shown. The *arrow* shows the direction of the flow. *Scale bar*, 10 μm.

whereby serine at 220 is mutated to alanine) and retrovirally expressed in PAE cells. Ser-220 mutation abrogated IGPR-1–dependent actin stress fiber rearrangement in response to shear stress (Fig. S5*B*). The data demonstrated that shear stress–induced phosphorylation of IGPR-1 at Ser-220 is required for actin stress fiber rearrangement in response to shear stress.

IGPR-1 is a mechanosensor receptor

Cell adhesion molecules, such as integrins, respond to mechanical cues such as stiffness of extracellular matrix (ECM) or forces generated from cell–cell interaction through cadherins and immunoglobulin-like cell adhesion molecules. We used tensile force (26) and atomic force microscopy (AFM) (27) to investigate the mechanosensor function of IGPR-1; these methods are commonly used to assess the effects of external forces on cells. The application of tensile force to IGPR-1 using magnetic beads was performed as previously described (28). For this, PAE cells expressing IGPR-1 were incubated with magnetic beads and coated with a mAb directed against the extracellular domain of IGPR-1 or mouse IgG as a control (Fig. 6*A*), and a constant force was applied for 15 min using a magnet. Following application of force, the cells were lysed, and whole-cell lysates were subjected to Western blotting analysis. Application of force selectively increased phosphorylation of IGPR-1 at Ser-220 (Fig. 6*B*) but not in cells incubated with control mouse IgG (Fig. 6*B*).

As an additional measure, we used AFM to examine the mechanosensing potential of IGPR-1. AFM is commonly used in various systems to study mechanotransduction (29). Fig. 6*C* shows representative indentation curves obtained from EV/PAE, IGPR-1/PAE, and A220–IGPR-1/PAE cells. To obtain the elastic modulus (*i.e.* the ratio of the force exerted on the membrane of PAE cells that results in deformation) of the cell membrane, the Hertz's model for nonadhesive elastic contact was used to correlate the loading force with indentation depth within the initial contact regime, spanning 0–25 pN force and up to 50 nm indentation depth (corresponding to ~10% of the total contact).

The elastic moduli obtained from different locations across the cell lines was plotted in the histograms (Fig. S6, *A* and *B*), and the statistics were determined (Fig. 6*D* and Table S1). These values are within the ranges of elastic moduli reported for other endothelial cells (30). There was a significant difference between the stiffness of IGPR-1/PAE and EV/PAE cells (*,

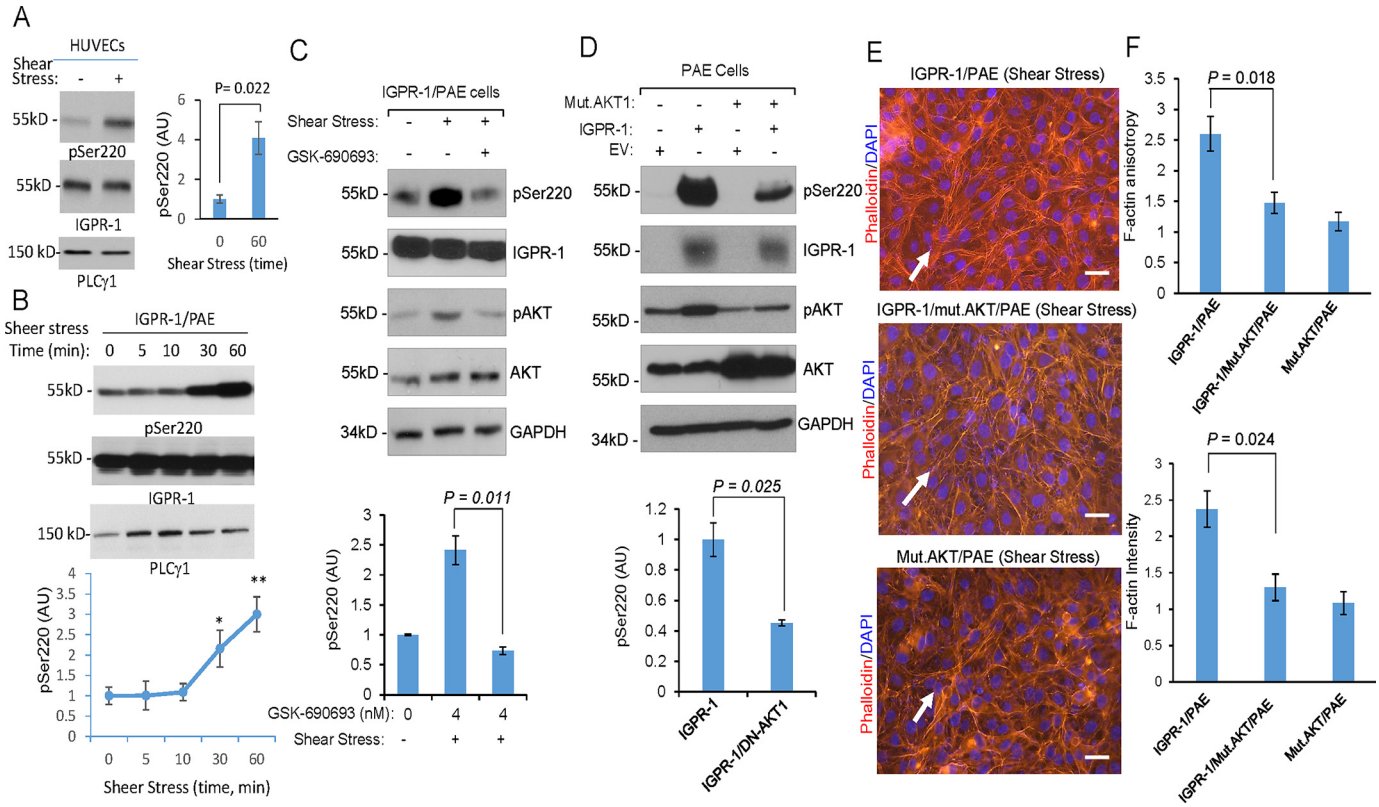

Figure 5. Shear stress–dependent phosphorylation of AKT mediates phosphorylation of IGPR-1. *A*, fully confluent HUVECs were kept in either normal static or under shear stress conditions. After 60 min, the cells were lysed, and whole-cell lysates were blotted for pSer-220, total IGPR-1, and PLCγ1. Shown is the normalized phosphorylation of Ser-220 to total IGPR-1, which is representative of three independent experiments. *B*, fully confluent IGPR-1/PAE cells were kept in normal static or under shear stress conditions for various times as indicated. The cells were lysed, and whole-cell lysates were blotted for pSer-220, total IGPR-1, and PLCγ1. The graph is representative of three independent experiments. Phosphorylation of Ser-220 was normalized to total IGPR-1. *C*, IGPR-1/PAE cells were incubated under shear stress in the presence of control vehicle or the pan-AKT inhibitor GSK-690693. The cells were lysed, and whole-cell lysates were blotted for pSer-220, IGPR-1, p-AKT, total AKT, and GAPDH. The graph is representative of three independent experiments. *D*, fully confluent PAE cells expressing EV, IGPR-1, mutant AKT1 (K179M/T308A/S473A) alone or co-expressed with IGPR-1 and mutant AKT1 were placed under shear stress for 6 h. The cells were lysed, and whole-cell lysates were blotted for pSer-220 (*pSer220*), total IGPR-1, AKT, and GAPDH. The graph is representative of three independent experiments. *E*, the fully confluent cell lines under static or shear stress were fixed and stained with phalloidin for actin (*red*) and DAPI (*blue*). *F*, F-actin orientation (anisotropy) and expression were quantified using an open source plugin Fibriltool. *Scale bar*, 10 μm. *Mut.*, mutant.

$p < 0.0001$) and between IGPR-1/PAE and A220–IGPR-1/PAE cells (**, $p = 0.0005$) (Fig. 6*D*). However, PAE cells expressing Ser-220 mutant IGPR-1 (A220–IGPR-1/PAE) showed lower stiffness. There was no statistically significant difference between the stiffness of EV/PAE and A220–IGPR-1/PAE cells ($p = 0.035$). The data suggest that phosphorylation of IGPR-1 likely through stimulation of stress fiber formation causes cells to become stiffer as measured by AFM.

Discussion

In this study, we demonstrated that IGPR-1 is activated by cell adhesion and shear stress, suggesting a mechanosensing function for this receptor in endothelial cells. The main function of blood vessels is to transport pressurized blood to tissues in the body, a process that exerts fluid shear stress on the endothelial cells (31, 32). Endothelial cells respond to and transduce the fluid shear stress from blood flow to biochemical signals that regulate endothelial cell morphology and gene expression through various mechanisms and pathways (31, 32), undergoing elongation and reorientation in the direction of flow as a result.

Although these physical properties are well-documented benchmarks of endothelial cells under flow shear stress, the molecular mechanisms responsible for promoting these effects are not fully understood. Our findings on IGPR-1 presented here shed further light into the processes governing endothelial cellular responses. IGPR-1 is expressed in both vein and arterial endothelial cells. However, its expression is higher in the arterial endothelial cells, suggesting a distinct function for IGPR-1 in the regulation of arterial endothelial cells. The endothelia of arterial and venous are distinctly different: arterial endothelial cells are generally thicker, and blood flow rates in the arterial circulation are significantly higher compared with venous endothelial cells and circulation (33). The salient feature of the arterial vessels is that the shear stress in the arterial vessels is significantly higher compared with veins (33). Our study demonstrates that IGPR-1, which is predominantly present at cell–cell contact areas, regulates actin stress fiber assembly and stabilizes cell–cell junctions. IGPR-1 localizes at adherens junctions in endothelial cells (10). Adherens junction serve multiple functions, including the regulation of cell–cell adhesion and control of the actin cytoskeleton fiber formation (34), suggesting a central role for IGPR-1 in the regulation of these cellular events. Additionally, IGPR-1 activity is regulated by endothelial cell spreading and adhesion because its phosphorylation was significantly increased in response to cell spreading

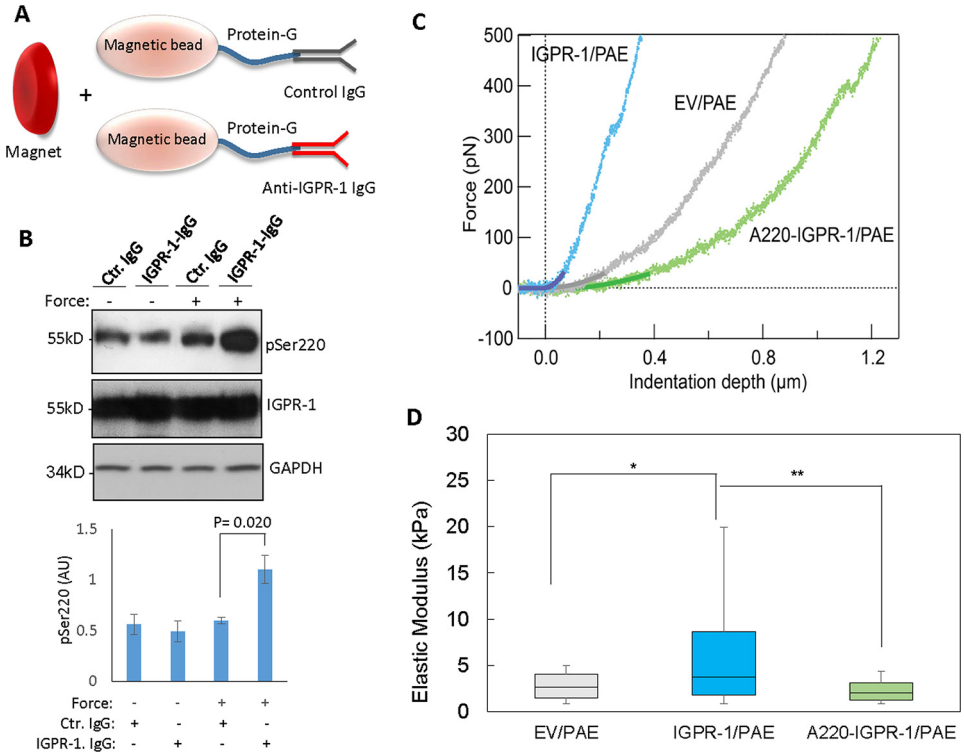

Figure 6. IGPR-1 regulates stiffness of endothelial cells. *A*, schematic of magnetic bead force assay is shown. *B*, cells were subjected magnetic bead force assay as described under "Materials and Methods." The cells were lysed and subjected to Western blotting analysis using pSer-220, total IGPR-1, and GAPDH antibodies. The graph is representative of three independent experiments. *C*, nanomechanical analysis carried out on the fully confluent PAE cells expressing empty vector, IGPR-1, or A220–IGPR-1 cultured on a glass slide. Representative nanoindentation curves on IGPR-1/PAE, EV/PAE, and A220–IGPR-1/PAE cells is shown. *D*, box plot of the cytoplasm elastic modulus for IGPR-1/PAE, EV/PAE, and A220–IGPR-1/PAE cells. The percentiles are 10, 25, 50, 75, and 90%. *, $p = 0.0001$; **, $p = 0.0005$. *Ctr.*, control.

and cell density. Considering that phosphorylation of IGPR-1 is regulated by homophilic transdimerization (10), it underscores the role of endothelial cell spreading and density in the activation of IGPR-1. Our study identifies AKT1 as a key kinase responsible for phosphorylating IGPR-1 at Ser-220, which is also activated by cell attachment and spreading (35). However, whether other kinases are also involved in phosphorylation of Ser-220 needs further investigation.

The important aspect of IGPR-1 expression in endothelial cells is its potential mechanosensing function. IGPR-1 is activated in response to shear stress and regulates actin stress fiber formation and realignment of endothelial cells. Flow-induced tension triggered IGPR-1 phosphorylation, which is mediated by AKT as in the presence of a dominant-negative AKT or the AKT inhibitor GSK-690693 phosphorylation of IGPR-1 in response to shear stress was greatly reduced. Indeed, direct application of tension via magnetic bead rapidly activated IGPR-1, further supporting the mechanosensing function of IGPR-1. Previous studies have shown that the phosphatidylinositol 3-OH-kinase/AKT pathway is activated by shear stress, which leads to activation of integrins (6).

Interestingly, phosphorylation of IGPR-1 in response to shear stress was slower (30 min) compared with phosphorylation of some proteins such as E-cadherin and integrins, which occurs in minutes. However, many other studies have shown that phosphorylation in response to shear stress was observed within the range of 30–60 min or longer. For example, maximum phosphorylation of AKT, eNOS (24, 36), and HDAC5 (37) were observed between 30 and 60 min. In this regard, IGPR-1 phosphorylation appears to be similar to these observations. Further evidence supporting the role of IGPR-1 as a mechanosensor protein obtained from nanomechanical characterization of PAE cells expressing IGPR-1 via AFM. PAE cells expressing IGPR-1 were significantly stiffer compared with control PAE cells or mutant Ser-220-IGPR-1, suggesting that expression of IGPR-1 in PAE cells altered the mechanical properties of PAE cells. In conclusion, the data presented in this study provide evidence for IGPR-1 as a mechanosensor receptor that is activated by shear stress and regulates shear stress–induced endothelial actin fiber assembly and endothelial realignment.

Materials and methods

Plasmids and antibodies

pBabe puro-Mutant Akt1 (K179M/T308A/S473A) was previously described (38), which was obtained from Addgene. Other plasmids including WT IGPR-1 and Ser-220 mutant IGPR-1 are previously described (10). Anti–IGPR-1 and pSer-220 antibodies are homemade antibodies and were previously described (10). Total AKT antibody and phospho-AKT antibody were purchased from Cell Signaling (Danvers, MA).

Cell culture

PAE cells expressing EV and PAE cells expressing IGPR-1 were maintained in DMEM supplemented with 10% fetal bovine serum and penicillin/streptomycin. HUVECs were purchased from ATCC and maintained in endothelial medium

(purchased from Lonza). Retroviruses were produced in 293-GPG cells as described (39).

Western blotting analysis

The cells were prepared and lysed, and whole-cell lysates were subjected to Western blotting analysis. Normalized whole-cell lysates were subjected to Western blotting analysis using IGPR-1 antibody or with appropriate antibody as indicated in the figure legends. Proteins were visualized using streptavidin–horseradish peroxidase–conjugated secondary antibody via the ECL system (Amersham Biosciences, GE Healthcare Bio-Sciences).

Flow shear stress

Fully confluent PAE cells expressing IGPR-1 or other constructs seeded in 60- or 100-mm plates were subjected to flow shear stress for various time points as indicated in the figure legends using an orbital shaker positioned inside an CO_2 incubator at 37 °C as previously described (40). The cells were either lysed and subjected to Western blotting analysis or fixed with 4% formaldehyde and subjected to immunofluorescence microscopy.

Immunofluorescence microscopy

PAE cells expressing IGPR-1 or other constructs were seeded (1.5×10^6 cells) onto coverslips and grown overnight in 60-mm plates to 90–100% confluence. In some experiments, the cells were placed on the orbital shaker in the CO_2 incubator and spun for various times as indicated in the figures legends. The cells were washed once with PBS and fixed with freshly prepared 4% paraformaldehyde for 15 min at room temperature. After washing three more times with PBS, the cells were permeabilized with 0.25% Triton X-100 in Western rinse for 10 min at room temperature and then washed three times with PBS. For actin staining, 0.20% rhodamine phalloidin (which stains actin) in PBS was added to the slides, incubated in a dark box for 10 min, and then washed twice with PBS. For localization of IGPR-1, the cells were blocked with (1:1) BSA in Western rinse for 1 h and washed once in PBS, followed with incubation with anti–IGPR-1 antibody (1:1000) for 1 h. After washing three times with 0.01% Tween 20 in Western rinse for 5 min each, rabbit FITC-conjugated secondary antibody was added for 1 h before being washed again in 0.01% Tween 20. The coverslips were mounted in Vectashield mounting medium with DAPI onto glass microscope slides. The slides were examined using a fluorescence microscope.

Quantification of F-actin stress fiber orientation and expression

PAE cells expressing IGPR-1 or other constructs were stained for actin as described above and visualized using an inverted epifluorescence microscope. From each image, we chose at random five different regions for evaluation. F-actin orientation (anisotropy) and expression were quantified using an open source plugin Fibriltool for ImageJ (22).

Magnetic bead force assay

The application of tensile force to IGPR-1 using magnetic beads was carried out as described (26). In brief, paramagnetic beads were coated with mouse anti–GPR-1 antibody or with control mouse antibody. 1.5 mg of Dynabeads–Protein G (Invitrogen) were coated with 10 μg of purified anti–IGPR-1 (1A12) or IgG. The beads were incubated with cells for 50 min at 37 °C followed by application of tensile forces to beads for 15 min using a permanent magnet. The magnet was placed parallel to and at a distance of 0.6 cm from the cell surface. After application of force, the cells were immediately lysed and subjected to Western blotting analysis.

Nanomechanical characterization

PAE cells expressing empty vector, IGPR-1, or A220–IGPR-1 were cultured on a glass slide until they reached to full confluence. The slides were washed twice with serum-free and filtered DMEM. The cells were kept in serum-free, filtered DMEM and immediately used for nanomechanical analysis. The AFM was performed using a MFP-3D microscope (Asylum Research, Santa Barbara, CA). An area scan was performed on the sample prior to the indentation experiment to locate the cells and its local density. The cell whose cytoplasm was in contact with its neighbor cells was selected to examine the effect of IGPR-1 at cell–cell contact region. The imaging was carried out in contact mode in serum-free and filtered DMEM at room temperature using a silicon nitride tip (Bruker AFM Probes, Camarillo, CA) with a nominal spring constant of 40 pN/nm. Force spectroscopy was obtained over a 250-nm extension length and a 500 nm/s approach and retreat velocity. Force curves (n = 100–256) were collected over an area of 10×10 μm. The set point was 500 pN. A thousand force curves were collected on 5–10 cells from different substrate areas to take into account the cell-to-cell variability. We distinguished force curves on the cell membrane from the bare substrate by the height difference and the apparent slope of the indentation curve, and the area scan performed right after the force map was carried out. To determine indentation depth, the cantilever's inverse optical lever sensitivity (m/V) was obtained by indenting the cantilever on a clean glass substrate. The glass substrate serves as an infinitely hard surface for determining the lever deflection response. Once an indentation was performed, the raw distance of the tip along the z-direction was converted into an indentation depth using the inverse optical lever sensitivity. The cantilever stiffness was determined from the thermal tuning method and compared with the manufacturer's specification. To quantify the cell cytoplasm's mechanical stiffness, Young's modulus, E, was determined from fitting the force curves using Hertz's model for nonadhesive elastic contact as described (18, 41). The Hertz's model assumes that the sample is homogeneous, perfect elastic and that there is no interaction between the tip and the substrate. The Hertz's model for nonadhesive elastic contact was used to determine the reduced elastic modulus as a result of the combined elasticities of the tip and sample by correlating the loading force, F, with indentation depth, δ.

$$F = \frac{2}{\pi} \frac{E_{\text{reduced}}}{1 - \nu^2} \delta^2 \tan(\alpha) \qquad \text{(Eq. 1)}$$

Here, ν is the Poisson ratio of the sample (set to 0.5 for a cell cytoplasm), and α is the half opening angle of the indenting tip

(21°). Finally, the sample modulus was calculated using the following equation.

$$\left(-\frac{1-\nu_{Tip}^2}{E_{Tip}}+\frac{1}{E_{reduced}}\right)^{-1}=\frac{E_{sample}}{1-\nu_{sample}^2} \quad \text{(Eq. 2)}$$

The tip's Young's modulus was set to 290 GPa, with a tip's Poisson ratio of 0.29 and a cone shape. Typical indentation curves display two regions with differing slopes. The initial contact regime (up to 50 nm of indentation depth), resulting from indentation of the cytoplasm surface, reflects the mechanical properties of the cell cytoplasm. As the tip penetrates deeper into the material, the underlying stiff substrate influences the mechanical response, altering the slope of the force curve. The data were fitted for indentation depths of up to 25 pN, corresponding to ~50–40 nm (10% of the total indentation depth). All analysis fitting was done using Igor Pro software (WaveMetrics Inc., Portland, OR).

Statistical analyses

The Student's two-tailed t test (assuming equal variances) was used to analyze cell survival data in experiments comparing two cell lines. For experiments that compared three or more cell lines, the one-way analysis of variance with Tukey's post hoc test was used to analyze the results. An α value of $p < 0.05$ denoted a significant difference between two groups. The statistical analysis of the cell stiffness was performed using an unpaired Student's t test with $p < 0.01$ denoted a significant difference.

Author contributions—R. X.-Y. H., R. T., and R. D. M. data curation; R. X.-Y. H., R. A., R. D. M., N. V., and N. R. formal analysis; R. X.-Y. H., R. T., R. A., R. D. M., and N. R. investigation; R. X.-Y. H. and N. R. writing-review and editing; R. A. methodology; R. D. M. validation; N. V. and M. G. software; N. V. visualization; M. G. and N. R. resources; M. G. and N. R. supervision; N. R. conceptualization; N. R. funding acquisition; N. R. writing-original draft; N. R. project administration.

References

1. Cavallaro, U., and Dejana, E. (2011) Adhesion molecule signalling: not always a sticky business. *Nat. Rev. Mol. Cell Biol.* **12,** 189–197 CrossRef Medline
2. Takahashi, M., Ishida, T., Traub, O., Corson, M. A., and Berk, B. C. (1997) Mechanotransduction in endothelial cells: temporal signaling events in response to shear stress. *J. Vasc. Res.* **34,** 212–219 CrossRef Medline
3. Noria, S., Cowan, D. B., Gotlieb, A. I., and Langille, B. L. (1999) Transient and steady-state effects of shear stress on endothelial cell adherens junctions. *Circ. Res.* **85,** 504–514 CrossRef Medline
4. Shay-Salit, A., Shushy, M., Wolfovitz, E., Yahav, H., Breviario, F., Dejana, E., and Resnick, N. (2002) VEGF receptor 2 and the adherens junction as a mechanical transducer in vascular endothelial cells. *Proc. Natl. Acad. Sci. U.S.A.* **99,** 9462–9467 CrossRef Medline
5. Bershadsky, A. D., Balaban, N. Q., and Geiger, B. (2003) Adhesion-dependent cell mechanosensitivity. *Annu. Rev. Cell Dev. Biol.* **19,** 677–695 CrossRef Medline
6. Tzima, E., Irani-Tehrani, M., Kiosses, W. B., Dejana, E., Schultz, D. A., Engelhardt, B., Cao, G., DeLisser, H., and Schwartz, M. A. (2005) A mechanosensory complex that mediates the endothelial cell response to fluid shear stress. *Nature* **437,** 426–431 CrossRef Medline
7. Orr, A. W., Helmke, B. P., Blackman, B. R., and Schwartz, M. A. (2006) Mechanisms of mechanotransduction. *Dev. Cell* **10,** 11–20 CrossRef Medline
8. Rahimi, N., Rezazadeh, K., Mahoney, J. E., Hartsough, E., and Meyer, R. D. (2012) Identification of IGPR-1 as a novel adhesion molecule involved in angiogenesis. *Mol. Biol. Cell* **23,** 1646–1656 CrossRef Medline
9. Woolf, N., Pearson, B. E., Bondzie, P. A., Meyer, R. D., Lavaei, M., Belkina, A. C., Chitalia, V., and Rahimi, N. (2017) Targeting tumor multicellular aggregation through IGPR-1 inhibits colon cancer growth and improves chemotherapy. *Oncogenesis* **6,** e378 CrossRef Medline
10. Wang, Y. H. W., Meyer, R. D., Bondzie, P. A., Jiang, Y., Rahimi, I., Rezazadeh, K., Mehta, M., Laver, N. M. V., Costello, C. E., and Rahimi, N. (2016) IGPR-1 is required for endothelial cell–cell adhesion and barrier function. *J. Mol. Biol.* **428,** 5019–5033 CrossRef Medline
11. Galbraith, C. G., Skalak, R., and Chien, S. (1998) Shear stress induces spatial reorganization of the endothelial cell cytoskeleton. *Cell Motil Cytoskeleton* **40,** 317–330 CrossRef Medline
12. Malek, A. M., and Izumo, S. (1996) Mechanism of endothelial cell shape change and cytoskeletal remodeling in response to fluid shear stress. *J. Cell Sci.* **109,** 713–726 Medline
13. Mierke, C. T. (2009) The role of vinculin in the regulation of the mechanical properties of cells. *Cell Biochem. Biophys.* **53,** 115–126 CrossRef Medline
14. Gardel, M. L., Schneider, I. C., Aratyn-Schaus, Y., and Waterman, C. M. (2010) Mechanical integration of actin and adhesion dynamics in cell migration. *Annu. Rev. Cell Dev. Biol.* **26,** 315–333 CrossRef Medline
15. Fanning, A. S., Jameson, B. J., Jesaitis, L. A., and Anderson, J. M. (1998) The tight junction protein ZO-1 establishes a link between the transmembrane protein occludin and the actin cytoskeleton. *J. Biol. Chem.* **273,** 29745–29753 CrossRef Medline
16. Tornavaca, O., Chia, M., Dufton, N., Almagro, L. O., Conway, D. E., Randi, A. M., Schwartz, M. A., Matter, K., and Balda, M. S. (2015) ZO-1 controls endothelial adherens junctions, cell–cell tension, angiogenesis, and barrier formation. *J. Cell Biol.* **208,** 821–838 CrossRef Medline
17. Schwarz, U. S., and Gardel, M. L. (2012) United we stand: integrating the actin cytoskeleton and cell-matrix adhesions in cellular mechanotransduction. *J. Cell Sci.* **125,** 3051–3060 CrossRef Medline
18. Sokolov, I., Dokukin, M. E., and Guz, N. V. (2013) Method for quantitative measurements of the elastic modulus of biological cells in AFM indentation experiments. *Methods* **60,** 202–213 CrossRef Medline
19. Steward, R., Jr, Tambe, D., Hardin, C. C., Krishnan, R., and Fredberg, J. J. (2015) Fluid shear, intercellular stress, and endothelial cell alignment. *Am. J. Physiol. Cell Physiol.* **308,** C657–C664 CrossRef Medline
20. Chowdhury, F., Na, S., Li, D., Poh, Y. C., Tanaka, T. S., Wang, F., and Wang, N. (2010) Material properties of the cell dictate stress-induced spreading and differentiation in embryonic stem cells. *Nat. Mater.* **9,** 82–88 CrossRef Medline
21. Ehrlicher, A. J., Nakamura, F., Hartwig, J. H., Weitz, D. A., and Stossel, T. P. (2011) Mechanical strain in actin networks regulates FilGAP and integrin binding to filamin A. *Nature* **478,** 260–263 CrossRef Medline
22. Boudaoud, A., Burian, A., Borowska-Wykret, D., Uyttewaal, M., Wrzalik, R., Kwiatkowska, D., and Hamant, O. (2014) FibrilTool, an ImageJ plug-in to quantify fibrillar structures in raw microscopy images. *Nat. Protoc.* **9,** 457–463 CrossRef Medline
23. Davies, P. F. (1995) Flow-mediated endothelial mechanotransduction. *Physiol. Rev.* **75,** 519–560 CrossRef Medline
24. Dimmeler, S., Assmus, B., Hermann, C., Haendeler, J., and Zeiher, A. M. (1998) Fluid shear stress stimulates phosphorylation of Akt in human endothelial cells: involvement in suppression of apoptosis. *Circ. Res.* **83,** 334–341 CrossRef Medline
25. Fisslthaler, B., Dimmeler, S., Hermann, C., Busse, R., and Fleming, I. (2000) Phosphorylation and activation of the endothelial nitric oxide synthase by fluid shear stress. *Acta Physiol. Scand.* **168,** 81–88 CrossRef Medline
26. Marjoram, R. J., Guilluy, C., and Burridge, K. (2016) Using magnets and magnetic beads to dissect signaling pathways activated by mechanical tension applied to cells. *Methods* **94,** 19–26 CrossRef Medline
27. Eyckmans, J., Boudou, T., Yu, X., and Chen, C. S. (2011) A hitchhiker's guide to mechanobiology. *Dev. Cell* **21,** 35–47 CrossRef Medline

28. Bays, J. L., Peng, X., Tolbert, C. E., Guilluy, C., Angell, A. E., Pan, Y., Superfine, R., Burridge, K., and DeMali, K. A. (2014) Vinculin phosphorylation differentially regulates mechanotransduction at cell–cell and cell–matrix adhesions. *J. Cell Biol.* **205,** 251–263 CrossRef Medline
29. Heinisch, J. J., Lipke, P. N., Beaussart, A., El Kirat Chatel, S., Dupres, V., Alsteens, D., and Dufrêne, Y. F. (2012) Atomic force microscopy: looking at mechanosensors on the cell surface. *J. Cell Sci.* **125,** 4189–4195 CrossRef Medline
30. Schaefer, A., and Hordijk, P. L. (2015) Cell-stiffness-induced mechanosignaling: a key driver of leukocyte transendothelial migration. *J. Cell Sci.* **128,** 2221–2230 CrossRef Medline
31. Paszkowiak, J. J., and Dardik, A. (2003) Arterial wall shear stress: observations from the bench to the bedside. *Vasc. Endovascular Surg.* **37,** 47–57 CrossRef Medline
32. Baeyens, N., Bandyopadhyay, C., Coon, B. G., Yun, S., and Schwartz, M. A. (2016) Endothelial fluid shear stress sensing in vascular health and disease. *J. Clin. Invest.* **126,** 821–828 CrossRef Medline
33. dela Paz, N. G., and D'Amore, P. A. (2009) Arterial versus venous endothelial cells. *Cell Tissue Res.* **335,** 5–16 CrossRef Medline
34. Hartsock, A., and Nelson, W. J. (2008) Adherens and tight junctions: structure, function and connections to the actin cytoskeleton. *Biochim. Biophys. Acta* **1778,** 660–669 CrossRef Medline
35. Zeller, K. S., Idevall-Hagren, O., Stefansson, A., Velling, T., Jackson, S. P., Downward, J., Tengholm, A., and Johansson, S. (2010) PI3-kinase p110α mediates β1 integrin-induced Akt activation and membrane protrusion during cell attachment and initial spreading. *Cell Signal.* **22,** 1838–1848 CrossRef Medline
36. Boo, Y. C., Hwang, J., Sykes, M., Michell, B. J., Kemp, B. E., Lum, H., and Jo, H. (2002) Shear stress stimulates phosphorylation of eNOS at Ser^{635} by a protein kinase A–dependent mechanism. *Am. J. Physiol. Heart Circ. Physiol.* **283,** H1819–H1828 CrossRef Medline
37. Wang, W., Ha, C. H., Jhun, B. S., Wong, C., Jain, M. K., and Jin, Z. G. (2010) Fluid shear stress stimulates phosphorylation-dependent nuclear export of HDAC5 and mediates expression of KLF2 and eNOS. *Blood* **115,** 2971–2979 CrossRef Medline
38. DiRenzo, J., Signoretti, S., Nakamura, N., Rivera-Gonzalez, R., Sellers, W., Loda, M., and Brown, M. (2002) Growth factor requirements and basal phenotype of an immortalized mammary epithelial cell line. *Cancer Res.* **62,** 89–98 Medline
39. Rahimi, N., Dayanir, V., and Lashkari, K. (2000) Receptor chimeras indicate that the vascular endothelial growth factor receptor-1 (VEGFR-1) modulates mitogenic activity of VEGFR-2 in endothelial cells. *J. Biol. Chem.* **275,** 16986–16992 CrossRef Medline
40. dela Paz, N. G., Walshe, T. E., Leach, L. L., Saint-Geniez, M., and D'Amore, P. A. (2012) Role of shear-stress-induced VEGF expression in endothelial cell survival. *J. Cell Sci.* **125,** 831–843 CrossRef Medline
41. Dokukin, M. E., Guz, N. V., and Sokolov, I. (2013) Quantitative study of the elastic modulus of loosely attached cells in AFM indentation experiments. *Biophys. J.* **104,** 2123–2131 CrossRef Medline